Available online at www.sciencedirect.com
SCIENCE DIRECT®
International Journal of Heat and Mass Transfer 47 (2004) 5257–5269
International Journal of HEAT and MASS TRANSFER
www.elsevier.com/locate/ijhmt

Fluid, heat and contaminant transport structures of laminar double-diffusive mixed convection in a two-dimensional ventilated enclosure

Qi-Hong Deng [a,*], Jiemin Zhou [a], Chi Mei [a], Yong-Ming Shen [b]

[a] School of Energy and Power Engineering, Central South University, Changsha, Hunan 410083, China
[b] State Key Lab of Costal and Offshore Engineering, Dalian University of Technology, Dalian 116023, China

Received 22 December 2003; received in revised form 11 June 2004
Available online 21 August 2004

Abstract

The objective of the present work is to investigate the characteristics of the airflow and heat/contaminant transport structures in the indoor air environment by means of a convection transport visualization technique. Laminar double-diffusive mixed convection in a two-dimensional displacement ventilated enclosure with discrete heat and contaminant sources is numerically studied. Based on the governing equations, the fluid, heat, and contaminant transport processes are respectively described by the corresponding streamfunction, heatfunction, and massfunction. Attentions are given to analyze the effects of the main factors—the strength of heat source indicated by the Grashof number (*Gr*), the strength of contaminant source by the buoyancy ratio (Br), the strength of ventilation by the Reynolds number (*Re*), and the ventilation mode—on the indoor air environment. Numerical results, presented by the contour function lines, namely, streamlines, heatlines, and masslines, illustrated that the indoor air, heat and contaminant transport structures are mainly determined by the interaction between the internal buoyancy natural convection induced by the discrete heat/contaminant sources and the external forced convection driven by the mechanical ventilation. It is found that the convection transport method could explicitly disclose the complicated philosophy of indoor air environment, and thus provides a simple but practical approach to see the indoor airflow and heat and contaminant transport structures.

Keywords: Transport structure; Double diffusion; Mixed convection; Displacement ventilation; Discrete heat/contaminant sources

1. Introduction

As people nowadays spend most of time indoors, indoor air environment (IAE) is receiving increasing concern for it is closely related to the health, comfort, and productivity of the occupants [1,2]. Compared to other industrial processes, indoor environment consists of more discrete heat and contaminant sources, such as pets, cooking, smoking, burning furnace, blazing window, office automation equipments, and building materials and furnishings, which intermittently or continuously produce allergens, heat, gas components (CO_2, CO, NO_x), particulate matter (PM_{10}, $PM_{2.5}$), and volatile organic compounds (VOCs) [3–6]. To

* Corresponding author. Fax: +86 731 8876554.
E-mail address: qhdeng@csu.edu.cn (Q.-H. Deng).

0017-9310/$ - see front matter © 2004 Elsevier Ltd. All rights reserved.
doi:10.1016/j.ijheatmasstransfer.2004.06.025

Nomenclature

Br	buoyancy ratio
c, C	dimensional and non-dimensional concentrations
D	mass diffusivity
g	gravity acceleration
Gr	Grashof number
h	sizes of inlet and outlet
H	height of ventilated room
l	length of heat/contaminant source
L	length of ventilated room
n	outward normal direction
Nu	average Nusselt number
p, P	dimensional and non-dimensional pressures
Pr	Prandtl number
Re	Reynolds number
Sc	Schmidt number
Sh	Sherwood number
t, T	dimensional and non-dimensional temperature
u, v	dimensional velocity components in x and y directions
U, V	non-dimensional velocity components in X and Y directions
x, y	dimensional coordinates
X, Y	non-dimensional coordinates

Greek symbols

α	thermal diffusivity
β	expansion coefficient
v	kinematic viscosity
ρ	density
Δt	temperature scale
Δc	concentration scale
ψ	stream function
ξ	heat function
ζ	mass function

Subscripts

i	inlet
h	high
c	concentration
t	temperature

control and/or remove these heat and contaminant so as to prevent them from doing harm to health, and also to provide thermal comfort, ventilation or air-conditioning is usually implemented as an indispensable measure. Two kinds of convection are involved in a ventilated room, i.e., internal buoyancy-induced natural convection by the discrete heat and contaminant sources and external mechanical-driven forced convection by the ventilation, which results in double-diffusive mixed convection. The indoor airflow and heat/contaminant transfer characteristics are therefore determined by the interaction between the natural convection and the forced one [7]. The double-diffusive mixed convection in ventilated enclosures with discrete heat and contaminant sources has also found wide applications in engineering, such as electronic cooling, chemical processing, thermal and pollution control, being the topic of the current research.

Mixed convection in enclosures with one isolated heat source, in which the interaction between an external forced flow and an internal buoyancy flow determines the fluid flow and heat transfer structures, has received considerable attentions in the last decade. Papanicolaou and Jaluria [8,9] numerically studied two-dimensional laminar mixed convection in a rectangular enclosure with a discrete heat source mounted on the wall. Two related studies of mixed convection in a partially divided rectangular enclosure were respectively carried out by Hsu et al. [10] and by How and Hsu [11]. The effect of an internal volumetric heat-generating and conducting solid body on the mixed convection in a square cavity was investigated by Yilbas et al. [12]. Laminar mixed convection in a two-dimensional enclosure heated from one sidewall and submitted to an either aiding or opposing jet was numerically studied in the work of Angirasa [13] and Raji and Hasnaoui [14]. The non-linear dynamical behaviors of mixed convection in a chemical vapor deposition (CVD) reactor and a ventilated room were respectively investigated by Santen et al. [15] and Chow et al. [16]. However, there are still various applications of mixed convection in enclosures due to multiple discrete heat sources (MDHSs). It is expected that the behavior of the total buoyancy natural convection flow induced by MDHSs is more complicated than that of the single buoyancy flow, and hence its interaction with the mechanical-driven forced convection. Only a few studies were found in the public literatures dealing with this aspect. Hsu and Wang [17] numerically examined a two-dimensional mixed convection in an enclosure with a separation board embedded with two equal discrete heat sources. Raji and Hasnaoui [18] investigated the mixed convection in ventilated cavities where the horizontal top wall and the vertical left wall were prescribed with equal heat fluxes.

By contrast with scarce study in enclosures, mixed convection due to MDHSs in channels has been intensively discussed. Mahaney et al. [19,20] both numerically and experimentally studied the effect of buoyancy-in-

duced flow on the forced flow in a three-dimensional horizontal channel with an array of 4×3 discrete heat sources mounted on the bottom wall. Yücel et al. [21] conducted a numerical study for mixed convection heat transfer in an inclined channel with discrete isothermal heating. In order to simulate the mixed convection occurring in multi-layered boards, Kim et al. [22] analyzed a horizontal channel with rectangular heating blocks attached on one side of the wall by imposing periodic boundary conditions on the horizontal walls. Bilen et al. [23] experimentally investigated the effect of the geometric position of wall mounted rectangular blocks on the mixed convection heat transfer in a rectangular channel, taking into account the angular displacement of the block in addition to its spanwise and streamwise disposition. Wang and Jaluria [24] numerically studied the three-dimensional mixed convection flow in a horizontal rectangular duct with MDHSs flush-mounted on the bottom surface, and main attention is focused on the characteristics of the instability and the resulting effect on the heat transfer. Hung and Fu [25] discussed the passive enhancement of mixed convection heat transfer in a horizontal channel with inner rectangular blocks by geometric modification.

Since heat and contaminant sources usually co-exist indoors, the present work is to numerically study the double-diffusive mixed convection in a ventilated enclosure due to the discrete heat and contaminant sources. As far as authors know, the problem has never been concerned in the public literatures, and therefore a detailed investigation is deserved to understand the indoor air environment. For the sake of simplicity and also as an initial endeavor, a two-dimensional laminar mixed convection with one discrete heat source and one discrete contaminant source is only considered here. However, without loss of generality, the method and the results could be straightforwardly extended to turbulent indoor air environment with multiple discrete heat and contaminant sources that may be involved in practice. The objective of the present work is to investigate the new characteristics of the airflow and heat/contaminant transport structures in indoor air environment by the simple and practical convection transport visualization technique in terms of streamlines, heatlines, and masslines [26–29].

2. Analysis

The physical model and the coordinate system under consideration are schematically shown in Fig. 1. It is a two-dimensional ventilated room of aspect ratio L/H. A heat source of size l and high temperature t_h, locates center on the left wall, and a contaminant source of equal size and high concentration c_h on the left part of the floor. A floor-based air-conditioning/displacement ventilation system is implemented, in which the low-speed fresh cold air (u_i, t_i, c_i) is supplied from the inlet at the bottom of right sidewall and then the polluted hot air exhausted from the top ceiling ($t_i < t_h$, $c_i < c_h$). The inlet and outlet are of the same size, h. Other parts of the enclosure are all considered adiabatic and impermeable.

Two kinds of convection are involved in above-mentioned ventilated room, one that the internal buoyancy-induced natural convection and the other external mechanical-driven forced convection. Meanwhile, the buoyancy force generated by the natural convection is

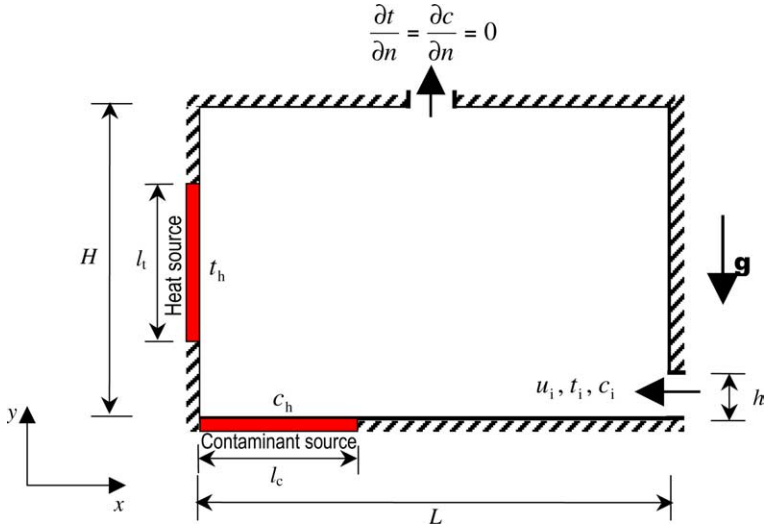

Fig. 1. Schematic of 2-D mixed convection in a displacement ventilated room.

in the same direction of ventilation or external forced convection, and thus the two convection mechanisms assist each other for the displacement ventilation system. However, for the traditional ventilation system, the fresh cold air is supplied from the top ceiling and exhausted from the bottom of the sidewall, i.e. a reversed flow as schematically shown in Fig. 1, where the internal natural convection is opposite to the external forced convection.

2.1. Governing equations

To simplify analysis, the following assumptions are made for the two-dimensional double-diffusive mixed convection: (1) the flow is steady, incompressible and laminar; (2) the air and the contaminant gases are perfectly mixed; (3) all the thermophysical properties of the fluid are constant, except for the density in the buoyancy term of the momentum equation following Boussinesq approximation.

Based on above assumptions, the governing equations are non-dimensionalized using H, u_i, Δt ($\Delta t = t_h - t_i$) and Δc ($\Delta c = c_h - c_i$) as characteristic scales for length, velocity, temperature and concentration respectively, as follows:

Continuity

$$\frac{\partial U}{\partial X} + \frac{\partial V}{\partial Y} = 0 \tag{1}$$

Momentum

$$\frac{\partial}{\partial X}(UU) + \frac{\partial}{\partial Y}(VU) = -\frac{\partial P}{\partial X} + \frac{1}{Re}\left(\frac{\partial^2 U}{\partial X^2} + \frac{\partial^2 U}{\partial Y^2}\right) \tag{2}$$

$$\frac{\partial}{\partial X}(UV) + \frac{\partial}{\partial Y}(VV) = -\frac{\partial P}{\partial Y} + \frac{1}{Re}\left(\frac{\partial^2 V}{\partial X^2} + \frac{\partial^2 V}{\partial Y^2}\right) + \frac{Gr}{Re^2}(T + \mathrm{Br}C) \tag{3}$$

Energy

$$\frac{\partial}{\partial X}(UT) + \frac{\partial}{\partial Y}(VT) = \frac{1}{RePr}\left(\frac{\partial^2 T}{\partial X^2} + \frac{\partial^2 T}{\partial Y^2}\right) \tag{4}$$

Concentration

$$\frac{\partial}{\partial X}(UC) + \frac{\partial}{\partial Y}(VC) = \frac{1}{ReSc}\left(\frac{\partial^2 C}{\partial X^2} + \frac{\partial^2 C}{\partial Y^2}\right) \tag{5}$$

where the dimensionless variables are $(X, Y) = (x, y)/H$, $(U, V) = (u, v)/u_i$, $P = p/\rho u_i^2$, $T = (t - t_i)/\Delta t$, $C = (c - c_i)/\Delta c$, and the dimensionless parameters are respectively $Re = u_i H/\nu$, $Gr = g\beta_t \Delta t H^3/\nu^2$, $\mathrm{Br} = \beta_c \Delta c/\beta_t \Delta t$, $Pr = \nu/\alpha$, $Sc = \nu/D$. In the present study, the thermal expansion coefficient β_t is positive for the density of the air mixture decreases as the temperature increases, and also $\beta_c > 0$ for the assumption that the polluted gas indoors is lighter than the air and thus the concentration of the air mixture decreases as the polluted gas increases, and hence $\mathrm{Br} > 0$. Therefore, the thermal buoyancy induced by heat source and the solutal buoyancy by contaminant source assist each other, and forms a combined buoyancy natural convection.

The boundary conditions of above governing equations for the considered problem are determined as:

Inlet: $U = -1$ and $V = 0$, $T = 0$, $C = 0$;
Outlet: $U = 0$ and $V = 1$, $\partial T/\partial \mathbf{n} = 0$, $\partial C/\partial \mathbf{n} = 0$;
Walls: $U = V = 0$, $T = 1$ for the heat source and $\partial T/\partial \mathbf{n} = 0$ elsewhere, $C = 1$ for the contaminant source and $\partial C/\partial \mathbf{n} = 0$ elsewhere.

The heat and mass transfer rates on the surfaces of heat and contaminant sources are described by the average Nusselt and Sherwood numbers, respectively, as follows

$$Nu = \int -(\partial T/\partial X)|_{X=0}\,\mathrm{d}Y \tag{6}$$

$$Sh = \int -(\partial C/\partial Y)|_{Y=0}\,\mathrm{d}X \tag{7}$$

2.2. Fluid, heat and mass transport

In order to clearly exhibit the fluid, heat and contaminant transport characteristics of double-diffusive mixed convection, a recently developed visualization technique of convective transport pathlines is employed. In terms of above continuity, energy, and concentration conversation equations, the streamfunction, heatfunction, and massfunction are respectively defined as follows:

Stream-function

$$-\frac{\partial \psi}{\partial X} = V, \quad \frac{\partial \psi}{\partial Y} = U \tag{8}$$

Heat-function

$$-\frac{\partial \xi}{\partial X} = VT - \frac{1}{RePr}\frac{\partial T}{\partial Y}, \quad \frac{\partial \xi}{\partial Y} = UT - \frac{1}{RePr}\frac{\partial T}{\partial X} \tag{9}$$

Mass-function

$$-\frac{\partial \zeta}{\partial X} = VC - \frac{1}{ReSc}\frac{\partial C}{\partial Y}, \quad \frac{\partial \zeta}{\partial Y} = UC - \frac{1}{ReSc}\frac{\partial C}{\partial X} \tag{10}$$

The corresponding contour lines, streamlines, heatlines, and masslines, are respectively representative of the transport pathlines of fluid, heat and contaminant.

2.3. Numerical procedures

Above governing equations are discretized by using a finite volume method (FVM) on a staggered grid system [30,31]. In the course of discretization, a third-order QUICK scheme and a second order central difference

are respectively implemented for the convection and diffusion terms. The resulting discretized equations are solved by a line-by-line procedure, combining the tri-diagonal matrix algorithm (TDMA) and the successive over-relaxation (SOR) iteration. The coupling between velocity and pressure is done by SIMPLE algorithm. The convergence criterion is that the maximal residual of all the governing equations is less than 10^{-6}.

In order to resolve the boundary layers along the surfaces of heat and contaminant sources, the grid was clustered toward the side walls. A systematic grid independence study was conducted, and the final grid resolution of 68×56 was selected at the balance between the calculation accuracy and the speed. The code used in the present work has been validated for many benchmark problems as given in [7,31,32].

3. Results and discussion

In the present study, the size configurations of the ventilated room, the heat and contaminant sources, and the inlet and outlet are kept constant as $L/H = 1.5$, $l/H = 0.5$, and $h/H = 1/8$. Both Prandtl number and Schmidt number are held fixed at 0.7. Main attention is then focused on the effects of the non-dimensional parameters, namely, Re, Gr, and Br, on the indoor air mixed convection. It is obvious that the Reynolds number (Re) is an indicative of the external forced convection or the strength of ventilation, the Grashof number (Gr) is a description of the strength of heat source, and the buoyancy ratio (Br) is representative of the strength ratio of contaminant source to heat source. Therefore, the indoor air environment is affected by three factors: the ventilation, the heat source, and the contaminant source.

3.1. Effect of Grashof number

To consider only the effect of Gr on the mixed convection, the other parameters are kept fixed at $Re = 500$ and Br = 1. Fig. 2 shows the variations of air, heat, and contaminant transport structures by streamlines, heatlines, and masslines as Gr increases. When the natural convection induced by the combined thermal and solutal buoyancy is very weak, $Gr = 10^3$ as shown in Fig. 2a, forced convection is the dominant transport mechanism. Therefore, the airflow pattern consists of one ventilated through-flow (open streamlines) and two induced clockwise and counter-clockwise secondary circulating flows respectively in the right and left parts of the room. The "V" shape heatlines and "N" shape masslines, respectively, show that the corresponding heat and contaminant are first transported downward by the left counter-clockwise induced flow and then carried out by the through-flow. The folded lines indicate that the removal efficiencies of heat and contaminant indoors are low. When natural convection increases to the level $Gr = 10^4$, as shown in Fig. 2b, the left counter-clockwise secondary flow is slightly weakened as seen that a small clockwise flow appears at the lower left corner due to the increasing combined thermal and solutal buoyancy effects. On the other hand, the front of the through-flow moves leftward as its induced counter-clockwise flow on the left side decreases. Accordingly, heatlines and masslines show an increasing diffusion effect near the heat and contaminant sources. The natural convection continues increasing with Grashof number, and its generated clockwise flow is expanded to a size comparable to that of the counter-clockwise cell induced by the forced convection when $Gr = 1.8 \times 10^4$, as shown in Fig. 2c. Heatlines and masslines show that heat and contaminant are first transported upward by the growing natural convection, then downward by the induced counter-clockwise cell, and finally taken out by the through-flow. As natural convection increases further, the clockwise natural convection flow expands and simultaneously the counter-clockwise induced flow shrinks, as a results the through-flow moving nearer and nearer to the left sidewall. It is found that when $Gr = 2.5 \times 10^4$, as shown in Fig. 2d, the natural convection flow is unified with the toward-coming through-flow, i.e., the natural convection with the forced convection. Affected by the flow structure, some amount of heat and contaminant is directly driven out by the unified upward flow in the left space, and the other amount is still affected by the counter-clockwise cell. Thus the heat and contaminant transport structures are of "Γ + V" and "Γ + N" shapes respectively, which indicate that the removal efficiency is improved as compared to the former folded "V" and "N" pathlines. Subsequently, the cooperation between the natural and forced convection is gradually enhanced as the natural convection increasing, which makes the counter-clockwise induced flow smaller and smaller and hence more and more heat and contaminant are transported directly outdoors. Fig. 2e and f shows that as $Gr \geqslant 10^5$, the combined buoyancy-induced natural convection is strong enough to dominate the flow structure. Streamlines show that the strong natural convection conducts the external air flowing towards the left wall along the floor, then upward along the left sidewall, and finally exiting from the outlet on the top ceiling, only one large clockwise secondary flow forming in the right part of the room. Heatlines and masslines show that heat and contaminant are directly swept off by the upward flow above the sources and hence of " Γ" shape transport structures. The short pathlines illustrate that heat and contaminant could be removed as soon as possible, which results in a high removal efficiency.

To illustrate the efficiency of heatlines and masslines visualizing heat and contaminant transport structures,

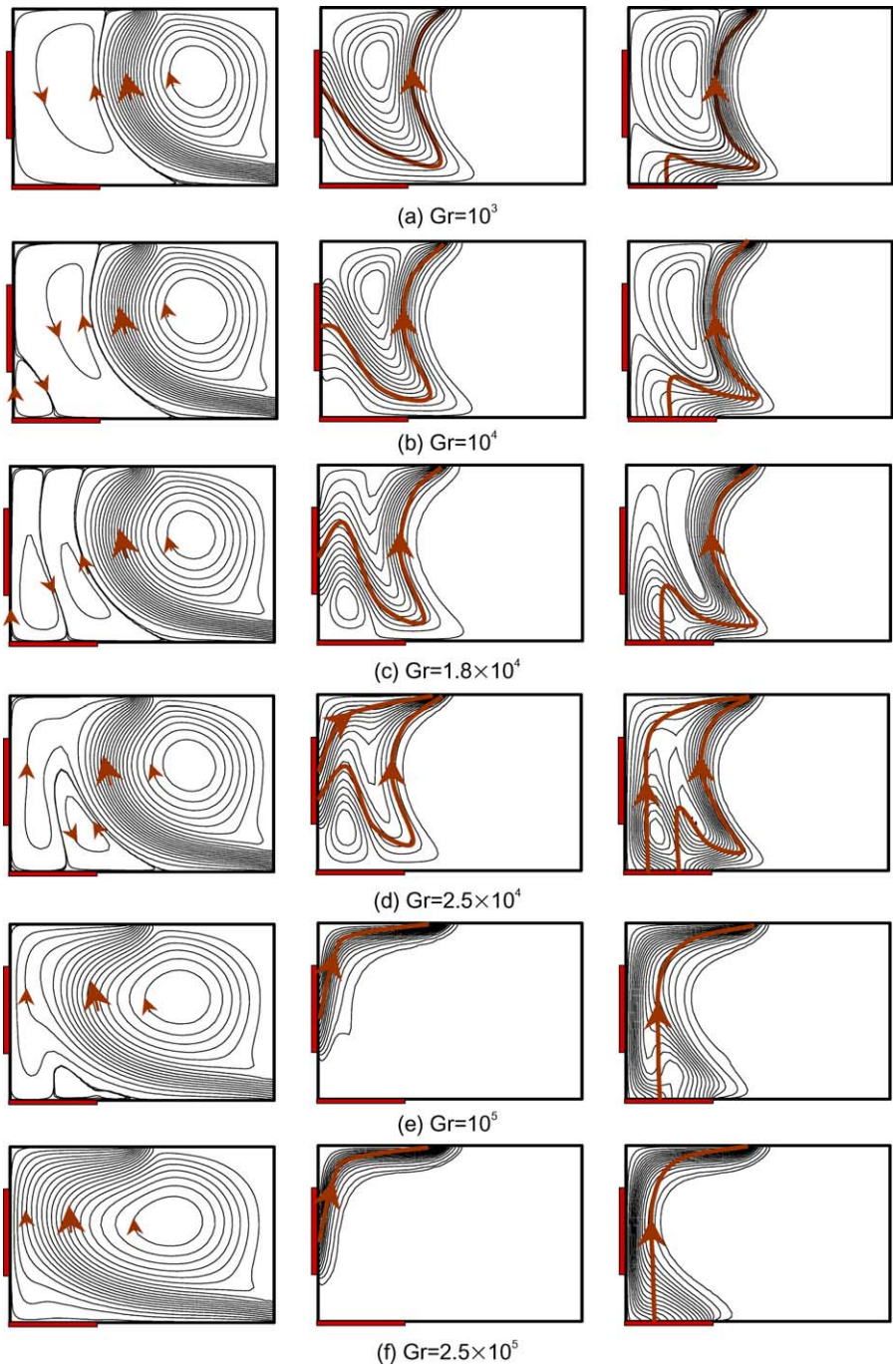

Fig. 2. Changes of fluid, heat and contaminant transport structures with Gr for $Re = 500$ (the heavy red lines and arrows schematically illustrate the main transport path and direction).

the traditional variations of average Nusselt and Sherwood numbers respectively for heat and contaminant sources in terms of Grashof number are plotted in Fig. 3. The parabolic curves illustrate that Nu and Sh first decrease slowly with increasing Gr, then reach minimum value at $Gr = 1.8 \times 10^4$, beyond which increase abruptly with increasing Gr. The reason is due to the fact that the competition between the buoyancy natural convection flow and the forced convection induced flow in the left space reaches maximum at the point $Gr = 1.8 \times 10^4$, as

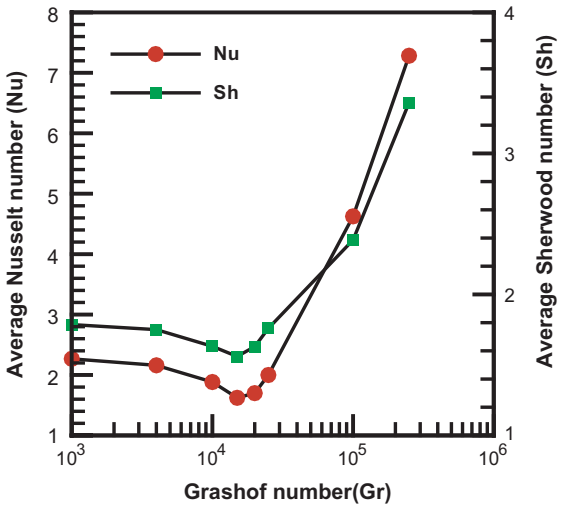

Fig. 3. Variations of *Nu* and *Sh* of heat and contaminant sources with *Gr* for *Re* = 500.

shown in Fig. 2c that heat and contaminant are first transported upward by the buoyancy flow and then downward by the ventilation induced flow and finally taken out of the room by the through-flow, the longest transport pathlines indicative of the lowest removal efficiency. Before that point, $Gr < 1.8 \times 10^4$, forced convection dominates the transport mechanism, and thus heat and contaminant are transferred mainly by the counterclockwise forced convection induced flow whose strength is however weakened gradually by the increasing buoyancy effect as *Gr* increasing. Therefore, both heat and mass transfer rates, *Nu* and *Sh*, decrease slowly. Beyond that point, $Gr > 1.8 \times 10^4$, natural convection wins the interaction with forced convection and hence dominates the transport mechanism, and therefore heat and contaminant are transferred mainly by the upward natural convection flow whose strength increases abruptly with increasing *Gr*. It is important to note from the variation curves of *Nu* and *Sh* that the mass transfer rate of the bottom contaminant source is globally smaller than the heat transfer rate of the left heat source, though two sources are of equal strength (Br = 1). The reason is due to the fact that the bottom source lies farther from the exhaust than the left heat source, and thus a longer transport path is required for contaminant removal, as indicated by the heatlines and masslines.

From above analysis, it is concluded that the heatlines and masslines provide a useful and simple means to visualize the heat and contaminant transport structures. From the pathlines, one can directly make a judge on the quality of indoor air environment. It is clearly found that increasing the strength of heat and contaminant sources in the left space are helpful for the heat and contaminant removal from indoors for the displacement ventilation system under consideration, which is contrary to the common sense that increasing the heat and contaminant sources would bring about more threat to health.

3.2. Effect of Reynolds number

From above analysis about the effect of Grashof number, it is observed that the fluid, heat and contaminant transport structures are determined by the interaction between the external forced convection and the internal buoyancy natural convection. To show the effect of Reynolds number, Fig. 4 plots the variations of *Nu* as the function of *Re* at different *Gr* levels. The general characteristics of the function are parabolic curves, such as the bolded curve *C* where $Gr = 10^4$, *Nu* first decreasing and then increasing with *Re*. The reasons are as follows: when the forced convection is weak, $Re < 400$, the buoyancy natural convection first dominates the airflow structure, and thus heat transfer decreases as the forced convection (*Re*) increases; the airflow pattern is however dominated by the external forced convection when $Re > 400$, and therefore heat transfer increases as *Re* increases; at $Re = 400$, the airflow structure is balanced by the two convection mechanisms, and thus heat transfer reaches the minimum. It is expected that when the strength of the internal buoyancy natural convection is weakened, such as the curve *B* ($Gr = 4 \times 10^3$), it will be easier for the external forced convection to dominate the flow structure, i.e. the parabolic curve moves towards left-side. When the buoyancy natural convection is much weakened to the level $Gr = 10^3$, curve *A*, the forced convection fully dominates the airflow structure, and thus heat transfer always increases as *Re* increases, i.e. the

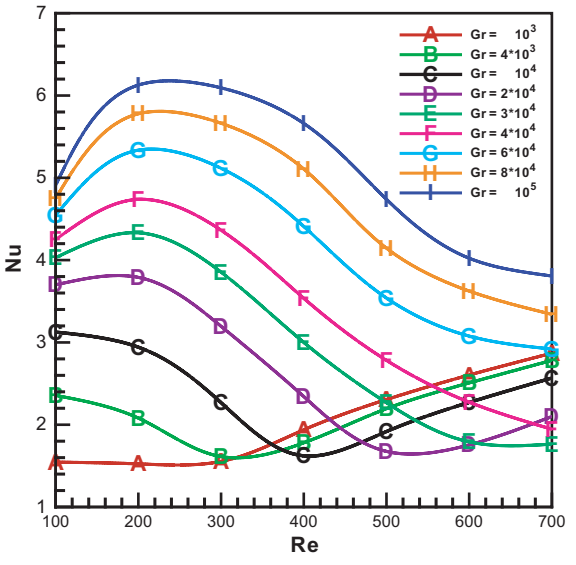

Fig. 4. Effects of *Re* on heat transfer rate for different *Gr*.

Nu–Re function is of monotonously increasing tendency or the right branch of the parabolic curve. On the contrary, when the natural convection is enhanced, such as the curve *D* ($Gr = 2 \times 10^4$), it will be harder for the forced convection to dominate the flow structure, and therefore the parabolic curve moves towards right-side. When the natural convection is further increased to $Gr \geqslant 4 \times 10^4$, curves *F–I*, the buoyancy natural convection fully dominates the airflow structure, and thus heat transfer decreases as *Re* increases, i.e. the *Nu–Re* function is basically of decreasing tendency or the left branch of the parabolic curve (note that when $Re < 200$, the ventilation flow is so small that the heat cannot be removed as soon as possible, and thus the heat transfer decreases as *Re* decreases). Fig. 5 shows the evolution of airflow structure with *Re* at different *Gr* levels. It confirms that: when the natural convection is weak, $Gr = 10^3$, there is only one possible state—the airflow dominated by the forced convection, and the counter-clockwise flow in the left part of room induced by the ventilation expands as *Re* increases, i.e. the dominance is augmented; when the natural convection is moderate, $Gr = 10^4$, there are three possible states—the airflow is first dominated by the natural convection, then by both natural convection and forced convection, and finally by the forced convection; when the natural convection is strong, $Gr = 6 \times 10^4$, there is again one state—airflow dominated by the natural convection, but its dominance is gradually weakened as the forced convection increases.

To deduce the resulting airflow structure, we need to know the relation between the natural convection and the forced convection. Above procedure implies that there is maximum competition between the internal natural convection and external forced convection, which results in minimum heat and contaminant transfer. The larger the forced convection (*Re*), the harder for the natural convection to compete with, or the larger value *Gr* is expected. Fig. 6 plots the correspondence between Grashof and Reynolds numbers when the minimum heat and contaminant transfer is reached. The relation between *Gr* and *Re* is linearly correlated by the

$$Re = 0.0125Gr + 272.41 \tag{11}$$

The region above the correlation curve is thus dominated by the forced convection, and natural convection dominates the region beneath the correlation curve.

From the curves of *Nu–Re*, one can also observe that when the buoyancy natural convection is weak ($Gr = 10^3$), increasing the forced convection or the ventilated flow would be beneficial to the heat and contami-

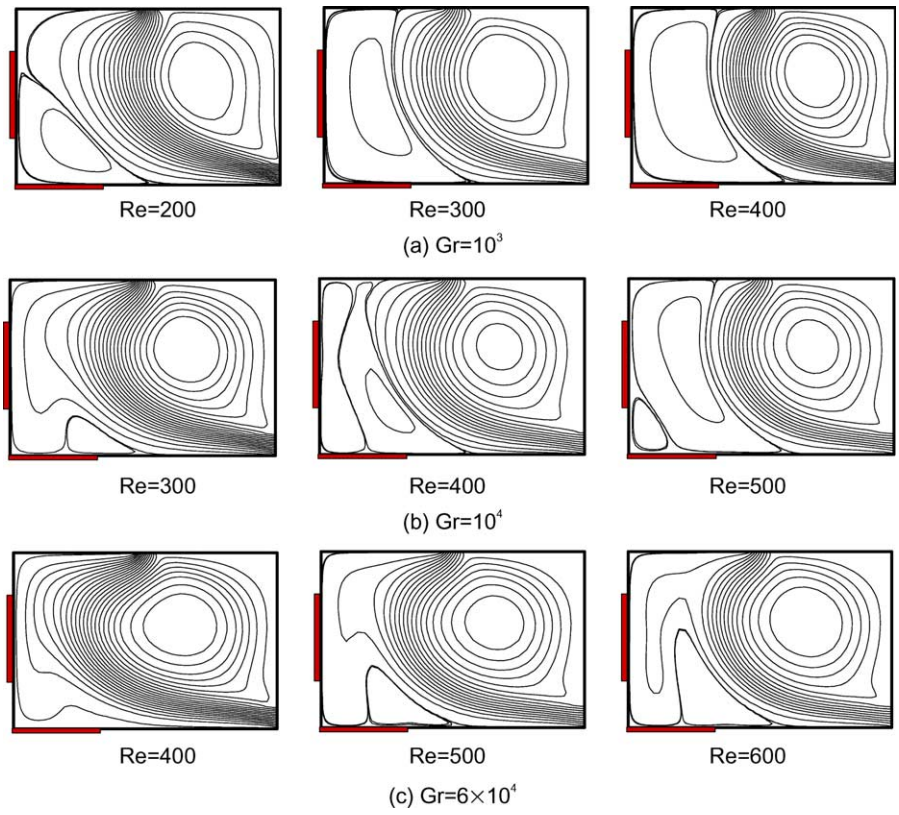

Fig. 5. Characteristics of fluid transport structures for different Grashof numbers.

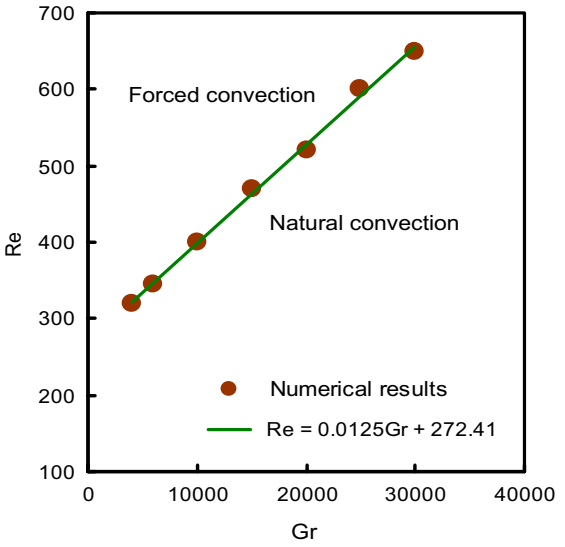

Fig. 6. The correlation between Gr and Re for minimization of Nu and Sh.

nant removal, however, it would degrade the removal efficiency when the buoyancy natural convection is strong ($Gr > 4 \times 10^4$). But at moderate buoyancy natural convection, the ventilation should be either increased or decreased in order to improve the heat and contaminant removal efficiencies. It should be noted that one cannot take it for granted that increasing the ventilation should be helpful to remove the heat and contaminant indoors.

3.3. Effect of buoyancy ratio

Fig. 7 shows the changes of fluid, heat and contaminant transport structures with Br for the case of $Re = 500$ and $Gr = 10^4$. The buoyancy ratio reflects the relative strength of contaminant source to heat source. When the left heat source described by Gr is kept fixed, the change of bottom contaminant source is represented by Br. For aiding thermal and solutal buoyancy effect, the total natural convection is increased when either buoyancy increases. Therefore, as Br increases, the airflow pattern changes from the first forced convection dominated structure, to the combined natural and forced convection structure, and finally to natural convection dominated structure. The corresponding heat transport structure changes from the beginning "V" shape to "Γ + V" shape and finally to "Γ " shape pathlines, and the contaminant transport pathlines change from the beginning "N" to "Γ + N" and finally to "Γ" shape.

Fig. 8 records the average Nusselt and Sherwood numbers for the case of $Re = 500$ and $Gr = 10^4$ at different buoyancy ratios within range of 0.1–10. It is again illustrated that the characteristics of heat and mass transfer are similar, which is due to the fact that when Br increases or equivalently the strength of contaminant

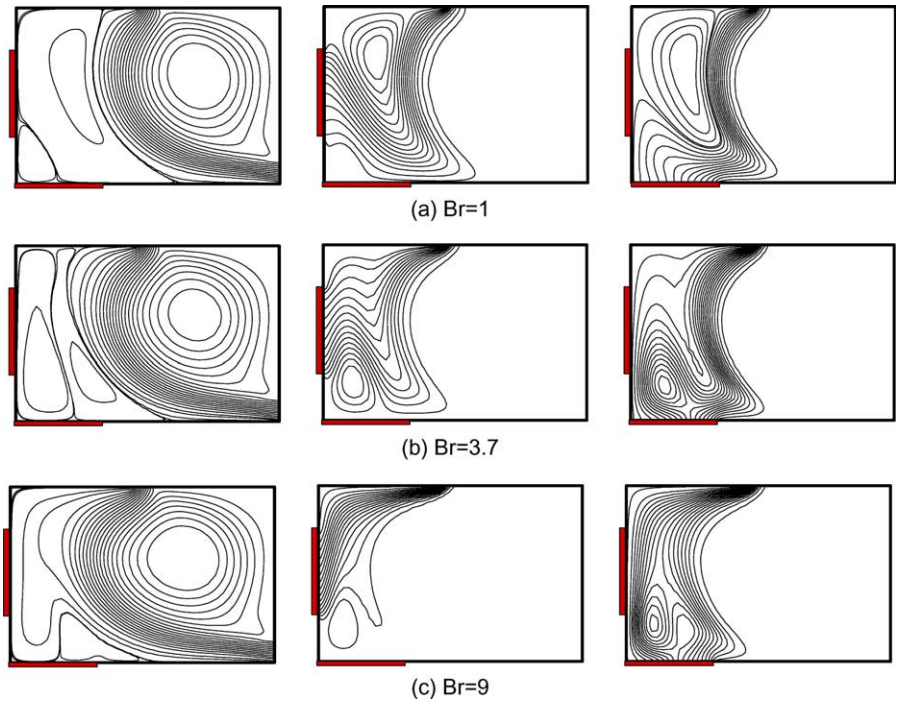

Fig. 7. Changes of fluid, heat and contaminant transport structures with Br for $Re = 500$ and $Gr = 10^4$.

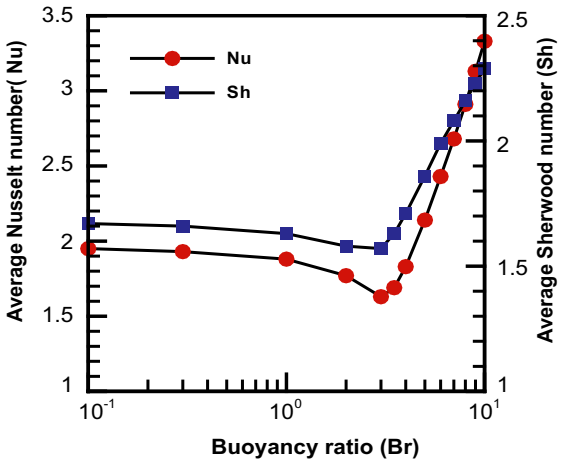

Fig. 8. Variations of *Nu* and *Sh* of heat and contaminant sources with Br ($Re = 500$ and $Gr = 10^4$).

source, the total natural convection increases. The variation profile indicates that the heat and mass transfer rates first decrease when $Br < 3.5$, where the airflow structure is dominated by the forced convection. But within the range of $0.1 < Br < 1$, the strength of the contaminant source is weaker than that of the heat source, and also the role of the former is weaker than the latter (as mentioned earlier), and therefore the heat and mass transfer are mainly determined by the left invariant heat source and hence invariant. When $1 < Br < 3.5$, the bottom contaminant source of the same order strength as the heat source, increasing the former means the total natural convection increases which degrades the effect of the forced convection, and thus the heat and mass transfer slowly decrease. At the point of $Br = 3.7$, the natural convection buoyancy-induced flow becomes a comparable force to that of the forced convection induced flow in the left space, and thus the heat and mass transfer reaches minimum. Beyond the point, when $Br > 3.5$, the airflow is dominated by the natural convection, and therefore the heat and mass transfer increase quickly with Br.

Fig. 9 shows airflow patterns at a lower and higher values of *Gr*, respectively 4×10^3 and 10^5, than the above-considered $Gr = 10^4$ at fixed $Re = 500$. It is found that when the left heat source is weakened, a much stronger bottom contaminant source is required for the combined natural convection to compete with the external forced convection. Fig. 9a shows that when $Br = 6$, the combined natural convection is still very weak compared to the forced convection, however it dominates the airflow pattern for $Gr = 10^4$ as shown in Fig. 7. Natural convection buoyancy-induced flow increases up to a comparable force to that of the forced convection induced flow until $Br = 11$ and then dominate the flow structure later at $Br > 20$. On the other hand, when the left heat source is increased strong enough, $Gr = 10^5$ as shown in Fig. 9b, its induced buoyancy natural convection is able to compete with the forced convection for any combination of the contaminant source.

It is obvious that, for assisting thermal and solutal buoyancy-induced natural convection pairs, one could be remedied by the other. A weak heat source could be appended by a strong contaminant source to compete with the external forced convection, or vice versa.

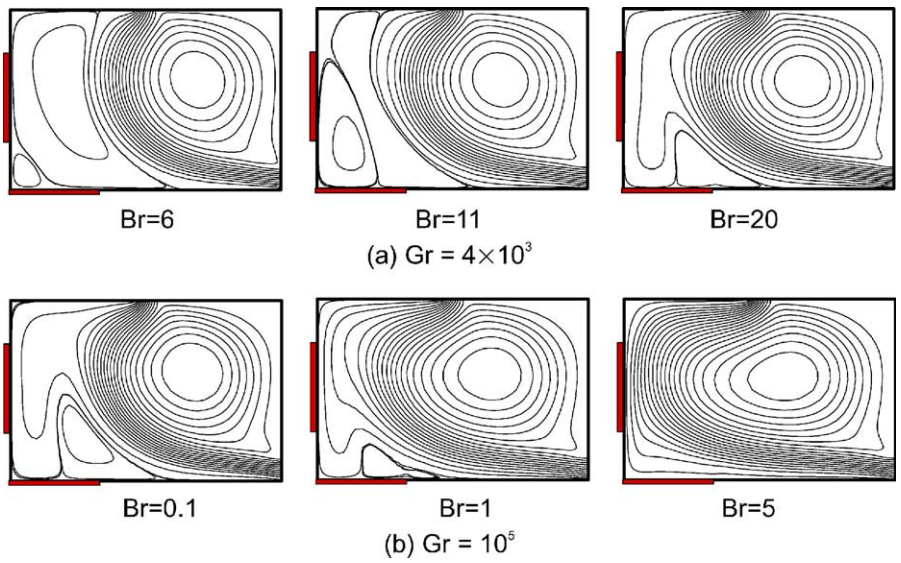

Fig. 9. Variations of Fluid transport structures with Br at different Grashof numbers ($Re = 500$).

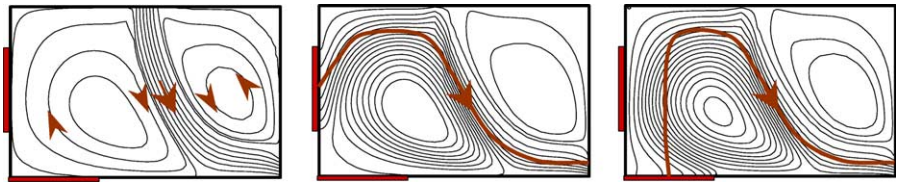

Fig. 10. Fluid (left), heat (center) and contaminant (right) transport structures with opposing natural and forced convection (Re = 500, $Gr = 10^4$, Br = 1).

3.4. Ventilation mode

As discussed before, for the displacement ventilation system, the natural convection assists the forced convection, and therefore the former acts a positive role in the task of heat and contaminant removal. In this way, the ventilation system can achieve the goal of maintaining a healthy indoor air environment at a low cost of the external forced convection whereby to save energy and also to reduce the noise. By contrast, the traditional ventilation system supplies the fresh cold air from the top ceiling and exhausts the polluted hot air from the bottom, a reversed flow pattern as schematically shown in Fig. 1. The airflow and heat/contaminant transport structures are shown in Fig. 10 under the conditions: $Gr = 10^4$, $Re = 500$, and Br = 1. Streamlines show that the natural convection in the left part causes the external forced convection skew towards the outlet, and therefore the space provided for the occupied people with cold/fresh air decreases. Heatlines and masslines indicate that the heat and contaminant are first conveyed upward by the buoyancy effect to the top ceiling and then downward by the strong external forced convection to the bottom outlet. The long and folded transportation paths imply very low heat/contaminant removal efficiency. On the other hand, the heat and contaminant transport paths run across the people occupied working zone and thus there is a risk. From the flow structures, we can deduce that when the natural convection increases, it would push the forced convection closer to the outlet. The forced convection would be 'short-circuiting' and thus nearly the full room would be in the circulating polluted hot airflow. Accordingly, the heatlines and masslines would run through the entire room. To avoid the 'lost of control' state, we have to increase the external forced convection. Therefore for the conventional ventilation system, natural convection becomes a burden of the external forced convection, so we have to increase the forced convection to eliminate the negative effect of the natural convection.

4. Conclusions

A two-dimensional laminar double diffusion mixed convection or displacement ventilation system is numerically investigated in the present work. The indoor air environment is mainly determined by the interaction between the internal buoyancy-induced natural convection by the discrete heat and contaminant sources and the external forced convection driven by the mechanical ventilation. The fluid, heat, and contaminant transport structures are described by the streamfunction/streamlines, heatfunction/heatlines, and massfunction/masslines respectively. Efforts has been concentrated on the effects of the main factors, namely Grashof number (Gr), buoyancy ratio (Br), Reynolds number (Re), and the ventilation mode, that influence the indoor air environment by the transport structures. Main conclusions are as follows:

(1) The streamlines, heatlines, and masslines provide a useful and simple means to visualize the fluid, heat, and contaminant transport structures. From the pathlines, one can directly make a judge on the quality of indoor air environment.
(2) As the combined buoyancy natural convection increases or equivalently the forced convection decreases, the indoor airflow changes from the first forced convection dominated structure, then to combined natural and forced convection structure, and finally to natural convection dominated structure. The corresponding heat transport structure changes from the beginning "V" shape then to "Γ + V" shape and finally to "Γ " shape pathlines, and the contaminant transport pathlines change from the beginning "N" then to "Γ + N" and finally to "Γ " shape. It is also found that only if the natural convection dominates the indoor airflow, increasing the strength of heat and contaminant sources are helpful for the heat and contaminant removal from indoors for the displacement ventilation.
(3) The airflow structure is determined by the relation between the internal natural convection and the external forced convection. The maximum competition between the two convection mechanisms which results in minimum heat and contaminant transfer is correlated by $Re = 0.0125Gr + 272.41$.
(4) When the buoyancy-induced natural convection is weak, increasing forced convection or the ventilated flow would be beneficial to the heat and contaminant removal, however, it would degrade the

removal efficiency when the buoyancy natural convection is strong. But at moderate buoyancy natural convection, the forced convection should be increased or decreased so as to improve the heat and contaminant removal efficiencies.

(5) For assisting thermal and solutal buoyancy-induced natural convection pairs, one could be remedied by the other. A weak heat source could be appended by a strong contaminant source to compete with the external forced convection, or vice versa.

(6) For assisting natural convection and forced convection, the former acts a positive role in the task of heat and contaminant removal and thus releases the requirement of the latter. But for the opposing effect, the natural convection becomes a burden of the forced convection.

Acknowledgments

This research is sponsored by the National Science Fund for Distinguished Young Scholars under Grant No. 50125924, the National Natural Science Foundation of China under Grant No. 50379001 and 50376076, and the Research Fund for the Doctoral Program of Higher Education under Grant No. 20010533009.

References

[1] J. Singh, Impact of indoor air pollution on health, comfort and productivity of the occupants, Aerobiologia 12 (1996) 121–127.

[2] W.J. Fisk, Health and productivity gains from better indoor environments and their relationship with building energy efficiency, Ann. Rev. Energy Environ. 25 (2000) 537–566.

[3] Ch. Monn, A. Fuchs, D. Högger et al., Particulate matter less than 10 μm (PM_{10})and find particles less than 2.5 μm ($PM_{2.5}$): relationships between indoor, outdoor and personal concentrations, Sci. Total Environ. 208 (1997) 15–21.

[4] C. Howard-Reed, L.A. Wallace, S.J. Emmerich, Effect of ventilation systems and air filters on decay rates of particles produced by indoor sources in an occupied townhouse, Atmos. Environ. 37 (2003) 5295–5306.

[5] R.G. Hamilton, P.A. Eggleston, Environmental allergen analysis, Methods 13 (1997) 53–60.

[6] P. Carrer, M. Maroni, D. Alcini, D. Cavallo, Allergens in indoor air: environmental assessment and health effects, Sci. Total Environ. 270 (2001) 33–42.

[7] Q.H. Deng, Modeling and Characteristics of Indoor Air Convection, PhD Thesis, Hunan University, Changsha, China, 2003.

[8] E. Papanicolaou, Y. Jaluria, Mixed convection from an isolated heat source in a rectangular enclosure, Numer. Heat Transfer, Part A 18 (1990) 427–461.

[9] E. Papanicolaou, Y. Jaluria, Mixed convection flow from a localized heat source in a cavity with conducting walls: a numerical study, Numer. Heat Transfer, Part A 23 (1993) 463–484.

[10] T.H. Hsu, P.T. Hsu, S.P. How, Mixed convection in a partially divided rectangular enclosure, Numer. Heat Transfer, Part A 31 (1997) 655–683.

[11] S.P. How, T.H. Hsu, Transient mixed convection in a partially divided enclosure, Comput. Math. Appl. 36 (1998) 95–115.

[12] B.S. Yilbas, S.Z. Shuja, M.O. Iqbal, Energy and entropy analysis in a square cavity with protruding body: effects of protruding body aspect ratio, Int. J. Energy Res. 26 (2002) 851–866.

[13] D. Angirasa, Mixed convection in a vented enclosure with isothermal vertical surface, Fluid Dyn. Res. 26 (2000) 219–233.

[14] A. Raji, M. Hasnaoui, Mixed convection heat transfer in a rectangular cavity ventilated and heated from the side, Numer. Heat Transfer, Part A 33 (1998) 533–548.

[15] H. Santen, C.R. Kleijn, H.E.A. Akker, On multiple stability of mixed convection flows in a chemical vapor deposition reactor, Int. J. Heat Mass Transfer 44 (2001) 659–672.

[16] C.K. Chow, G. Xin, S. Liu, Multiple attractors of mixed convection in confined spaces, Numer. Heat Transfer, Part A 39 (2001) 471–485.

[17] T.H. Hsu, S.G. Wang, Mixed convection in a rectangular enclosure with discrete heat sources, Numer. Heat Transfer, Part A 38 (2000) 627–652.

[18] A. Raji, M. Hasnaoui, Mixed convection heat transfer in ventilated cavities with opposing and assisting flows, Eng. Comput. 17 (2000) 556–572.

[19] H.V. Mahaney, S. Ramadhyani, F.P. Incropera, Numerical simulation of three-dimensional mixed convection heat transfer from an array of discrete heat sources in a horizontal rectangular duct, Numer. Heat Transfer, Part A 16 (1989) 267–286.

[20] H.V. Mahaney, F.P. Incropera, S. Ramadhyani, Comparison of predicted and measured mixed convection heat transfer from an array of discrete sources in a horizontal rectangular channel, Int. J. Heat Mass Transfer 33 (1990) 1233–1245.

[21] C. Yücel, M. Hasnaoui, L. Robillard, E. Bilgen, Mixed convection heat transfer in open ended inclined channels with discrete isothermal heating, Numer. Heat Transfer, Part A 24 (1993) 109–126.

[22] S.Y. Kim, H.J. Sung, J.M. Hyun, Mixed convection from multiple-layered boards with cross-streamwise periodic boundary conditions, Int. J. Heat Mass Transfer 35 (1992) 2941–2952.

[23] K. Bilen, S. Yapici, C. Celik, A Taguchi approach for investigation of heat transfer from a surface equipped with rectangular blocks, Energy Conver. Manage. 42 (2001) 951–961.

[24] Q. Wang, Y. Jaluria, Instability and heat transfer in mixed convection flow in a horizontal duct with discrete heat sources, Numer. Heat Transfer, Part A 42 (2002) 445–463.

[25] T.C. Hung, C.S. Fu, Conjugate heat transfer analysis for the passive enhancement of electronic cooling through geometric modification in a mixed convection domain, Numer. Heat Transfer, Part A 35 (1999) 519–535.

[26] A. Bejan, Convection heat transfer, Wiley, New York, 1995.
[27] V.A.F. Costa, Unified streamline, heatline, and massline methods for the visualization of two-dimensional heat and mass transfer in anisotropic media, Int. J. Heat Mass Transfer 46 (2003) 1309–1320.
[28] Q.H. Deng, G.F. Tang, Numerical visualization of mass and heat transport for conjugate natural convection/heat conduction by streamline and heatline, Int. J. Heat Mass Transfer 45 (2002) 2373–2385.
[29] Q.H. Deng, G.F. Tang, Numerical visualization of mass and heat transport for mixed convective heat transfer by streamline and heatline, Int. J. Heat Mass Transfer 45 (2002) 2387–2396.
[30] S.V. Patankar, Numerical heat transfer and fluid flow, Hemisphere, Washington, DC, 1980.
[31] Q.H. Deng, G.F. Tang, Special treatment of pressure correction based on continuity conservation in a pressure-based algorithm, Numer. Heat Transfer, Part B 42 (2002) 73–92.
[32] Q.H. Deng, G.F. Tang, Y. Li, M.Y. Ha, Interaction between discrete heat sources in horizontal natural convection enclosures, Int. J. Heat Mass Transfer 45 (2002) 5117–5132.